

# Remote RF Powering System for Wireless MEMS Strain Sensors

Nattapon Chaimanonart, *Student Member, IEEE*, and Darrin J. Young

**Abstract**—A reliable remote radio frequency (RF) powering system is developed for industrial wireless microelectromechanical systems (MEMS) strain-sensing applications. The prototype system is insensitive to mechanical rotation and produces a stable DC voltage of 2.8 V with a 2-mA current supply capability from a 50-MHz RF power source with a power conversion efficiency of 11%. An improved efficiency can be expected with an optimized power transmitter design. The CMOS power converter electronics are fabricated in a 1.5- $\mu\text{m}$  CMOS process occupying an area of approximately  $1 \times 1$  mm. The achieved DC power is adequate for supplying a high-performance wireless MEMS strain-sensing system.

**Index Terms**—Inductive coupling, microelectromechanical systems (MEMS) microsystems, radio frequency (RF) powering system, strain sensors, telemetry.

## I. INTRODUCTION

HIGH-PERFORMANCE strain-sensing microsystems consisting of miniature sensors and integrated interface electronics are highly desirable for advanced industrial applications, such as point-stress and torque sensing for ball bearings, rotating shafts and blades, etc. The sensed information is important for optimizing system performance, understanding material fatigue, and achieving reliable system monitoring and intelligent control. Stringent performance requirements with a high sensitivity of 0.1 micro-strain ( $\mu\epsilon$ ) over a wide signal bandwidth of 10 kHz and a large dynamic range of 80 dB are typically demanded for these applications. Industrial strain sensing further imposes significant design challenges due to various rotating mechanical components employed in a system. Therefore, stand-alone wireless-sensing microsystems with remote powering and data telemetry capabilities are highly desirable. Inductive-coupling-based powering techniques have been widely used for biomedical implants [1]–[4]. In these applications, an external radio frequency (RF) power source drives a coil loop, which couples the RF energy into an implanted miniature coil through magnetic coupling to power the microelectronics. The same wireless link can be also used for data telemetry. These coupling coils, however, are fixed at certain positions with a short distance on the order of a few millimeters. It is, therefore, necessary to develop remote powering techniques, which are insensitive to mechanical rotations

Manuscript received October 1, 2004; revised June 10, 2005. This work was supported by the U.S. Army Research Office (ARO) under contract DADD19-02-1-0198. The associate editor coordinating the review of this paper and approving it for publication was Prof. Ignacio Matias.

The authors are with the Department of Electrical Engineering and Computer Science, Case Western Reserve University, Cleveland, OH 44106-7221 USA (e-mail: nxc35@case.edu; djy@po.cwru.edu).

Digital Object Identifier 10.1109/JSEN.2006.870158

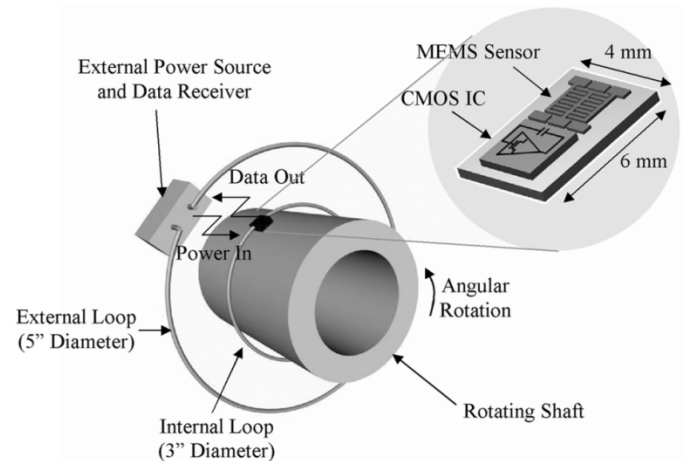


Fig. 1. Wireless microsystem architecture.

and can achieve an increased coupling distance for advanced industrial-sensing applications. In this paper, an RF remote powering system, consisting of rotation-insensitive coupling coil loops and integrated CMOS power converter electronics, is presented to obtain a stable DC voltage of 2.8 V with a 2-mA current supply capability from a 50-MHz RF operation. The available DC power is adequate for supplying a high-performance strain-sensing microsystem achieving a sensing dynamic range of 81 dB with a strain resolution of  $0.09 \mu\epsilon$  over a 10-kHz bandwidth. The demonstrated system performance represents two orders of magnitude improvement compared to any existing commercial strain sensor technologies, critical for advanced high-performance applications. Section II presents the proposed wireless microelectromechanical systems (MEMS) strain-sensing system and remote RF powering architecture. The integrated CMOS power converter electronics design is described with system design specifications in Section III with the overall system performance evaluation results shown in Section IV.

## II. REMOTE RF POWERING ARCHITECTURE

Fig. 1 presents the overall wireless microsystem architecture, which consists of a MEMS capacitive strain sensor and integrated CMOS interface and power conversion electronics, coupled with two coil loops for remote powering and data telemetry. The microsystem occupies an area of approximately  $4 \times 6$  mm including packaging and is attached to the surface of a rotating iron shaft with a diameter of 3 in. An internal coil is wound around the shaft and separated from the external coil by one inch for the prototype design. This configuration is critical for achieving a stable and uniform magnetic coil coupling

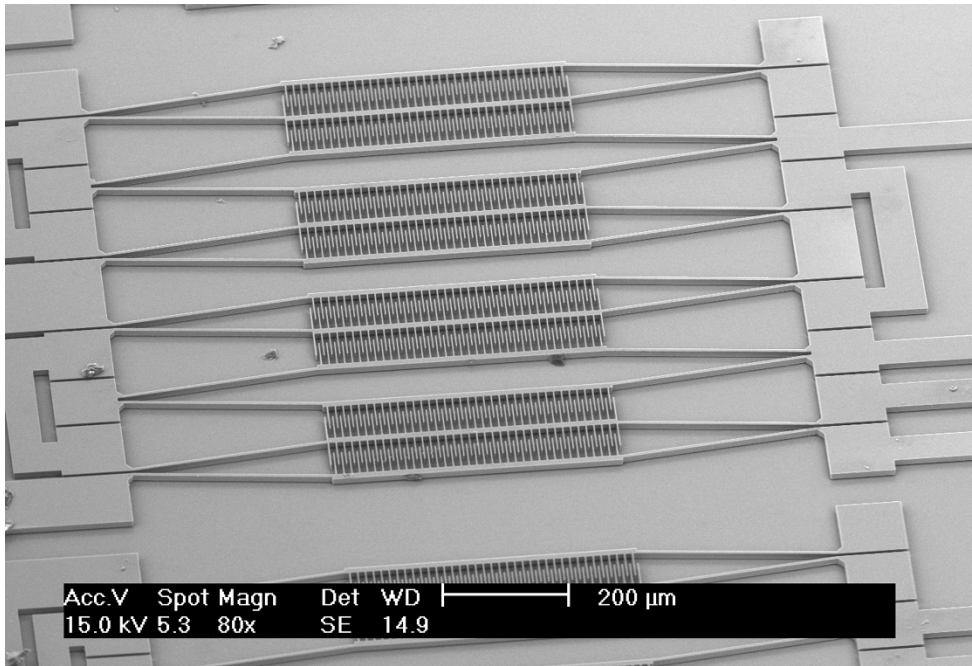


Fig. 2. SEM photo of a fabricated silicon MEMS capacitive strain sensor.

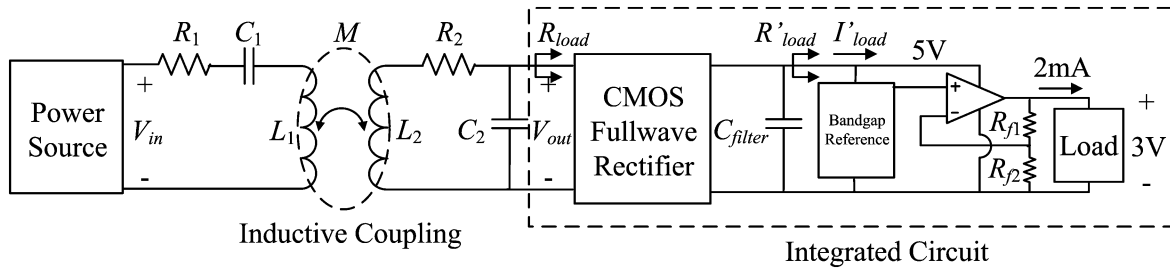


Fig. 3. Remote RF powering architecture.

during shaft rotation; hence, a stable power conversion for supplying the wireless microsystem. The rotation of the shaft produces a rotational torque, thus, a surface strain which can be sensed by the MEMS strain sensor. Fig. 2 shows an SEM photo of a fabricated silicon MEMS capacitive strain sensor developed in our research group [5], which exhibits a gauge length of 1 mm and a nominal sensor capacitance value of 440 fF with a differential sensitivity of 265 aF/ $\mu\epsilon$ , employed for the prototype design. The sensor output can be converted to a voltage, followed by digitization and data telemetry to a nearby receiver for signal acquisition and analysis. Fig. 3 presents the proposed remote RF powering architecture, where an external RF power source is used to drive a tuned series resonator consisting of  $L_1$  and  $C_1$ . The resistor  $R_1$  represents the overall series resistance associated with the resonator including the output resistance of the power source. The resonator is tuned to an optimal frequency as will be illustrated in Section III. The RF signal is coupled to a parallel resonator, consisting of  $L_2$  and  $C_2$  with a total loop resistance of  $R_2$ , tuned to the same frequency. The signal is then rectified by an integrated CMOS fullwave rectifier to 5 V and further regulated to achieve a stable 3-V DC supply with a 2-mA current driving capability, as a design specification, to power the overall microsystem illustrated in Fig. 1.

In order to achieve an efficient power conversion system, the voltage gain across the tuned resonator networks needs to be maximized. The gain can be expressed as

$$\frac{V_{out}}{V_{in}} = \frac{\omega^2 L_2 M}{\left( R_1 R_2 + (\omega M)^2 + \frac{R_1 (\omega L_2)^2}{R_{load}} \right)} \quad (1)$$

where  $M$  represents the mutual inductance between the two coil inductors:  $L_1$  and  $L_2$ ,  $\omega$  is the operating frequency, and  $R_{load}$  is the equivalent resistive loading presented to the parallel resonator by the CMOS fullwave rectifier, which can be determined as [6]

$$R_{load} = \frac{R'_{load}}{\sqrt{2}} \quad (2)$$

where  $R'_{load}$  is the resistive loading at the fullwave rectifier output and is approximately equal to 2 k $\Omega$  due to a 2.5 mA of the loading current  $I'_{load}$  at the 5-V line. This then results in a resistance of 1.4 k $\Omega$  for  $R_{load}$ . In the prototype design,  $R_1$  exhibits 12  $\Omega$ , which is dominated by the output resistance of the power source. All other parameters in (1),  $L_1$ ,  $L_2$ ,  $M$ , and  $R_2$ , are a function of coil turn number and operating frequency. These parameters have been extensively characterized to obtain

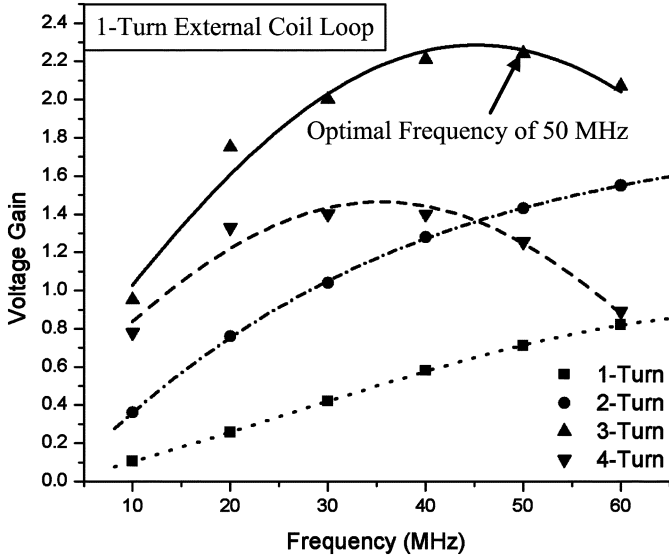


Fig. 4. Measured voltage gain frequency response with internal coil turn numbers.

an optimal condition for achieving a maximum voltage gain. Fig. 4 presents the measured voltage gain as a function of frequency and coil turn number, which closely matches the predicted performance from (1). It can be seen that a maximum voltage gain of 2.25 can be achieved at a 50-MHz operating frequency by employing a one-turn external coil loop, exhibiting an inductance value of 320 nH and high-frequency resistance of 0.8  $\Omega$ , and a three-turn internal coil loop with an inductance value of 450 nH and high-frequency resistance of 9.4  $\Omega$ . The high-frequency resistance of the three-turn internal coil loop made by using the same gauge wire is mainly caused by the iron core loss associated with the 50-MHz operation near the core surface. Both coil loops have self resonant frequencies well above 100 MHz and exhibit a mutual inductance of 25 nH. A design employing a four-turn internal coil loop suffers from a low voltage gain due to an excessive iron core loss at high frequencies. The one-turn external coil is chosen due to its simplicity. Furthermore, experiments have shown that a design with a two-turn external coil can achieve a comparable gain. However, a much reduced operating frequency is required, limited by the self resonant frequency of the external coil. The reduced frequency will call for an excessively large on-chip filter capacitor, as will be illustrated in Section III, to achieve a desired output voltage ripple requirement and, thus, is unsuitable for microsystem implementation. The measurement results also reveal that the voltage gain would drop from its maximum value of 2.25 to 1.7 with a tilting angle of 30° between the two coils due to a reduced mutual coupling. The proposed characterization and design approach can be adapted for shafts made of different materials to achieve an optimal performance.

### III. INTEGRATED CMOS POWER CONVERTER ELECTRONICS

An integrated CMOS fullwave rectifier is used to rectify the received RF signal. Fig. 5 presents the rectifier schematic, where  $V_{AC-Input}$  represents the coupled RF signal across the parallel resonator, which is to be rectified to produce a DC

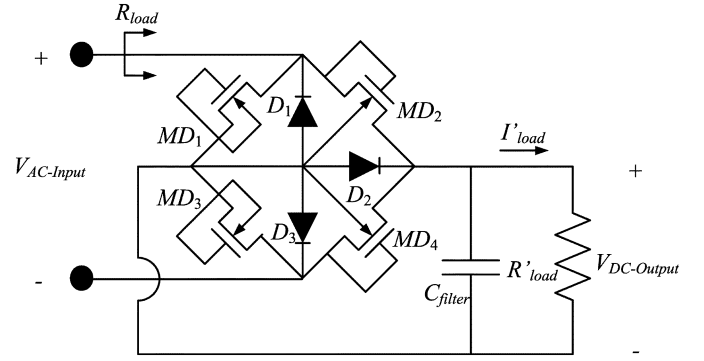


Fig. 5. Fullwave rectifier.

output voltage,  $V_{DC-Output}$ . The four MOSFET's connected in a diode configuration,  $MD_1$ ,  $MD_2$ ,  $MD_3$ , and  $MD_4$ , along with their parasitic source and drain to bulk junction diodes,  $D_1$ ,  $D_2$ , and  $D_3$ , form the fullwave rectifier. In a half cycle,  $MD_2$  and  $D_3$  perform the rectification with  $MD_4$  and  $D_1$  conducting during the other half cycle. The diode  $D_2$  does not cause any performance degradation since it is always kept in a reverse bias condition. The total voltage drop across the rectifier is approximately 2.7 V, of which 2 V is consumed by the MOSFET diode due to an increased threshold voltage caused by body effect, and 0.7 V is dropped over the junction diode. Therefore, an RF signal with a 7.7-V amplitude is required to obtain a rectified DC output voltage of 5 V. A filtering capacitor  $C_{filter}$  needs to be properly selected in order to achieve a certain ripple requirement as shown in (3)

$$C_{filter} = \frac{\pi \cdot I'_{load}}{V_r \omega} \quad (3)$$

where  $V_r$  is the peak-to-peak ripple voltage amplitude,  $I'_{load}$  is the DC loading current at the rectifier output, and  $\omega$  is the RF operating frequency. Thus, an increased operating frequency is desirable for achieving a low ripple with a reduced filtering capacitor size. The prototype wireless microsystem design specification calls for a peak-to-peak ripple voltage of 60 mV at the 5-V line; thus, a 400-pF filtering capacitor, occupying a chip area of approximately 0.9  $\times$  0.9 mm, is required with  $I'_{load}$  of 2.5 mA. The maximum AC peak current flowing through the fullwave rectifier can be approximately five to ten times larger than  $I'_{load}$  [7]. Device characterization shows that the maximum junction current density for the CMOS technology employed for the prototype design is around 8  $\mu A/\mu m^2$ . Therefore, a conservative source and drain to bulk junction area of 616  $\times$  34  $\mu m$  is chosen for  $MD_1$ ,  $MD_2$ ,  $MD_3$ , and  $MD_4$  to achieve a reliable operation.

Fig. 6 presents the schematic of a CMOS linear regulator used in the prototype system. The regulator holds the output voltage at a desired value of 3 V by comparing the output, through a resistive feedback network consisting of  $R_{f1}$  and  $R_{f2}$ , to a stable bandgap reference voltage  $V_{ref}$  of 1.25 V [8] with a high-gain inverting amplifier. Resistance values of 7 and 5 k $\Omega$  for  $R_{f1}$  and  $R_{f2}$ , respectively, are chosen to obtain a proper feedback ratio of 2.4. Furthermore, these resistor values are selected as a compromise considering the feedback network DC power dissipation, output regulation performance, and system

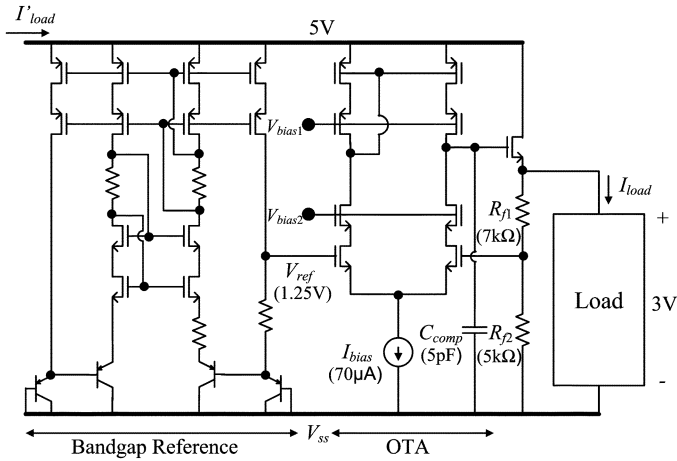


Fig. 6. CMOS linear regulator.

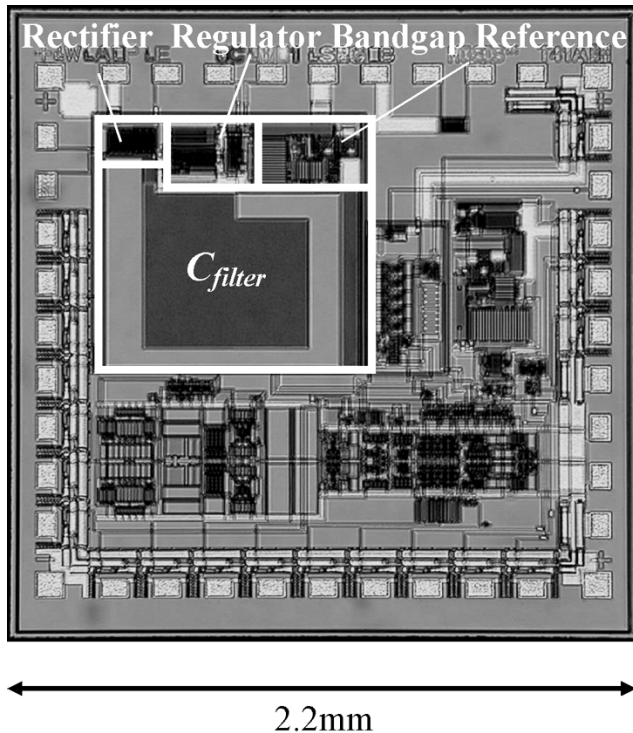


Fig. 7. Chip micrograph.

noise contribution. An output load resistance of  $1.5 \text{ k}\Omega$  is used throughout the design process to ensure a 2-mA current driving capability. A telescopic architecture with a large output swing is selected for the operational transconductance amplifier (OTA). From linear system analysis, it can be shown that the ripple rejection ratio from the 5-V line to the 3-V output is inversely proportional to the DC gain of the amplifier. Therefore, the OTA is designed with a low-frequency gain of 60 dB and a unity gain frequency of 20 MHz set by the compensation capacitor  $C_{comp}$  of 5 pF to achieve a rejection ratio of  $-20 \text{ dB}$ , which is adequate for the overall microsystem performance requirements. The CMOS regulator output noise is typically dominated by the reference voltage noise since the OTA and resistive feedback network can be designed with a negligible noise contribution. In the prototype design, the bandgap reference output voltage

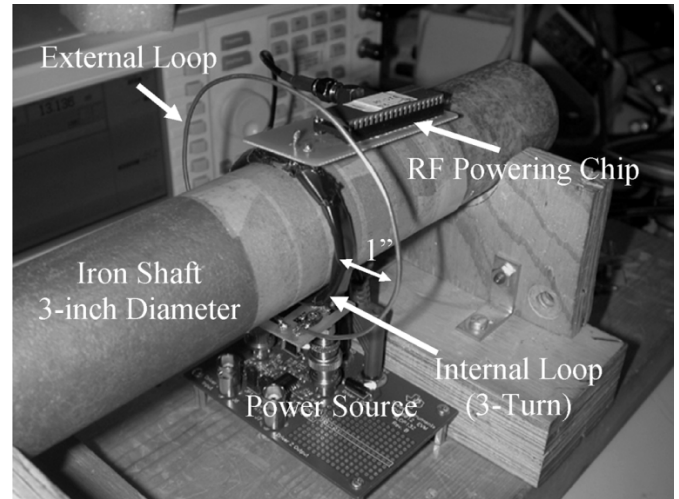


Fig. 8. Test setup.

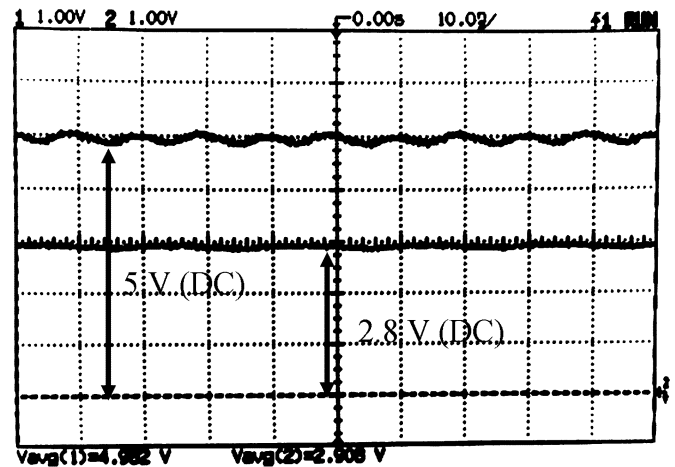


Fig. 9. 5- and 2.8-V DC outputs.

noise spectral density is designed to be  $112 \text{ nV}/\sqrt{\text{Hz}}$  by correct choice of the devices' dimensions, thus resulting in a regulator output noise floor of  $269 \text{ nV}/\sqrt{\text{Hz}}$ , which is adequate for the proposed wireless microsystem application.

#### IV. MEASUREMENT RESULTS

The integrated CMOS power converter electronics are fabricated in a  $1.5\text{-}\mu\text{m}$  CMOS process. Fig. 7 shows a photograph of the IC, where the converter occupies an area of approximately  $1 \times 1 \text{ mm}$  and is also integrated with the low-noise MEMS strain sensor detection electronics. The test setup for the prototype remote RF powering system is shown in Fig. 8. A 50-MHz RF power source with an amplitude of 8-V peak-to-peak is used to drive the tuned LC network. The CMOS chip is packaged in a through-hole DIP40 package mounted on the surface of an iron shaft. The system provides a stable DC voltage of 2.8 V with a 2-mA current supply capability independent of the iron shaft rotation, thus achieving a power conversion efficiency of 11%. An improved efficiency can be expected with an optimized power transmitter design [9]. The regulator output exhibits a line regulation and load regulation of 4.8 mV/V and 0.96 mV/mA, respectively. Fig. 9 shows the voltage

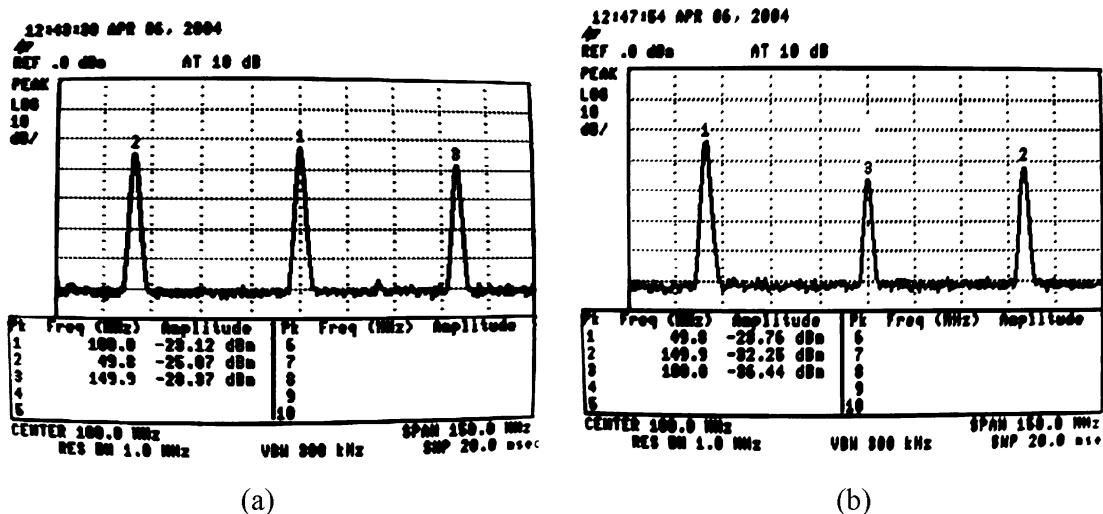


Fig. 10. Measured spectrum at (a) 5-V line and (b) 2.8-V output.

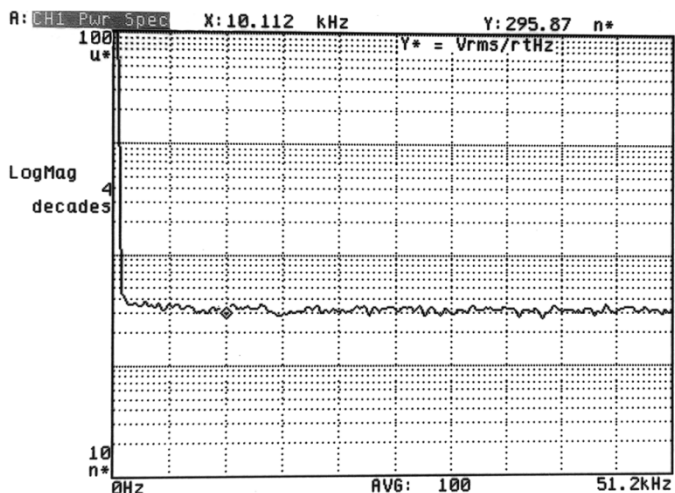


Fig. 11. Noise spectral density at 2.8-V output.

waveforms at the 5-V line and 2.8-V output. The regulated output voltage deviates from the designed value of 3 V due to the reference voltage,  $V_{\text{ref}}$ , being 1.2 V instead of the designed value of 1.25 V, which is caused by the lack of accurate p-n junction model for the parasitic pnp devices used in the bangap reference design. The 5-V line and 2.8-V output exhibit a ripple amplitude of 203- and 82-mV peak-to-peak, respectively, which are larger than the expected values. Further spectrum analysis indicates that the increased ripple amplitude is caused by a strong package coupling at 50 MHz. Fig. 10 presents the measured spectrum at the 5-V line and 2.8-V output. It can be seen that the 5-V line exhibits two strong tones: a 50-MHz tone with a power of approximately  $-25$  dBm (equivalent to a 80-mV peak-to-peak amplitude based on calibration) and a 100-MHz tone with  $-23$ -dBm power (equivalent to a 100-mV peak-to-peak amplitude). The 2.8-V output contains a strong 50-MHz tone with a similar power level as that at the 5-V line and a 100-MHz tone with a reduced power level of  $-36$  dBm (equivalent to a 20-mV peak-to-peak amplitude). It is clear that the 50-MHz signal is due to the coupling of the package

used for the system characterization, which can be significantly suppressed with an improved package for the final system design. The expected 100-MHz tone exhibits a suppression of approximately  $-13$  dB from the 5-V line, which is comparable to the designed value of  $-20$  dB. The discrepancy is likely caused by the on-chip substrate coupling. An improved on-chip layout isolation technique such as grounded guard rings can be employed to further enhance the performance. The CMOS regulator output achieves a low-noise performance. Fig. 11 presents the measured noise spectral density with a noise floor of  $296$  nV/ $\sqrt{\text{Hz}}$ , which closely matches the designed value of  $269$  nV/ $\sqrt{\text{Hz}}$  with a difference of 0.8 dB. After completing the electrical characterization, the remote RF powering system is used to power the MEMS strain sensor and integrated low-noise interface electronics to achieve superior performance: a minimum detectable strain of  $0.09$   $\mu\epsilon$  over a 10-kHz bandwidth and a dynamic range 81 dB. This is the same performance achieved by using a 3-V battery power supply [10]. The demonstrated microsystem performance represents two orders of magnitude improvement compared to existing commercial strain-sensing technologies.

## V. CONCLUSION

A reliable remote RF powering system for advanced industrial MEMS strain-sensing application is presented. The prototype system is designed to be insensitive to mechanical rotations and outputs a stable DC voltage of 2.8 V with a 2-mA current supply capability from a 50-MHz RF operation. The power converter electronics are integrated with the low-noise strain sensor interface circuitry and can provide a sufficient power to a wireless strain-sensing microsystem to demonstrate a superior performance.

## REFERENCES

- [1] J. A. Von Arx and K. Najafi, "A wireless single-chip telemetry-powered neural stimulation system," in *Proc. IEEE Int. Solid-State Circuits Conf.*, Feb. 1999, pp. 214–215.
- [2] W. Liu and M. S. Humayun, "Retinal prosthesis," in *Proc. IEEE Int. Solid-State Circuits Conf.*, Feb. 2004, pp. 218–225.

- [3] J. Ji and K. D. Wise, "An implantable CMOS circuit interface for multiplexed microelectrode recording arrays," *IEEE J. Solid-State Circuits*, vol. 27, no. 3, pp. 433–443, Mar. 1992.
- [4] B. Smith, Z. Tang, M. W. Johnson, S. Pourmehdi, M. M. Gazdik, J. R. Buckett, and P. H. Peckham, "An externally powered, multichannel, implantable stimulator-telemeter for control of paralyzed muscle," *IEEE Trans. Biomed. Eng.*, vol. 45, no. 4, pp. 463–475, Apr. 1998.
- [5] J. Guo, H. I. Kuo, D. J. Young, and W. H. Ko, "Buckled beam linear output capacitive strain sensor," in *Proc. Solid-State Sensor, Actuator, Microsystems Workshop*, Jun. 2004, pp. 344–347.
- [6] Z. Tang, B. Smith, J. H. Schild, and P. H. Peckham, "Data transmission from an implantable biotelemetry by load-shift keying using circuit configuration modulator," *IEEE Trans. Biomed. Eng.*, vol. 42, no. 5, pp. 524–528, May 1995.
- [7] A. R. Hambley, *Electronics*, 2nd ed. NJ: Prentice Hall, 2000.
- [8] P. R. Gray and R. G. Meyer, *Analysis and Design of Analog Integrated Circuits*, 3rd ed. New York: Wiley, 1993.
- [9] P. R. Troyk and G. A. DeMichele, "Inductively-coupled power and data link for neural prostheses using a class-E oscillator and FSK modulation," in *Proc. IEEE Int. Conf. Engineering Medicine Biology Soc.*, vol. 4, Sep. 2003, pp. 3376–3379.
- [10] M. Suster, J. Guo, N. Chaimanonart, W. H. Ko, and D. J. Young, "Low-noise CMOS integrated sensing electronics for capacitive MEMS strain sensors," in *Proc. IEEE Custom Integrated Circuits Conf.*, Oct. 2004, pp. 693–696.



**Nattapon Chaimanonart** (S'04) received the B.S. degree in engineering from the Electrical Engineering Department, Chulalongkorn University, Bangkok, Thailand, in 2001. Currently, he is pursuing the Ph.D. degree at Case Western Reserve University, Cleveland, OH, where Prof. D. J. Young is his Research Advisor.

His research interests include integrated circuit design for wireless communications and interface electronics for biomedical sensing applications.



**Darrin J. Young** received the B.S., M.S., and Ph.D. degrees from the Department of Electrical Engineering and Computer Sciences, University of California, Berkeley, in 1991, 1993, and 1999, respectively. His doctoral dissertation emphasized on microelectromechanical devices design and fabrication technologies for radio frequency analog signal processing.

Between 1991 and 1993, he was with Hewlett-Packard Laboratories, Palo Alto, CA, where he designed a shared memory system for a DSP-based multiprocessor architecture. During the summer of 1997, he was with Rockwell Semiconductor Systems, Newport Beach, CA, where he designed silicon bipolar RF analog circuits for cellular telephony applications. Between 1997 and 1998, he was with Lawrence Livermore National Laboratory, Livermore, CA, working on the design and fabrication of three-dimensional RF MEMS coil inductors for wireless communications. He joined the Department of Electrical Engineering and Computer Science, Case Western Reserve University, Cleveland, OH, in 1999, where he is currently an Associate Professor. His research interests include MEMS and nanoelectromechanical devices design, fabrication, and integrated analog circuit design for sensing, communications, biomedical implants, and general industrial applications.